Available online at www.sciencedirect.com
SCIENCE DIRECT®
Journal of Sound and Vibration 290 (2006) 264–289
JOURNAL OF SOUND AND VIBRATION
www.elsevier.com/locate/jsvi

SEA substructuring using cluster analysis: The MIR index

N. Totaro*, J.L. Guyader

Laboratoire Vibrations Acoustique, INSA de Lyon, Bâtiment St. Exupéry, 20, Avenue Albert Einstein, 69621 Villeurbanne Cedex, France

Received 22 December 2003; received in revised form 31 January 2005; accepted 31 March 2005
Available online 1 September 2005

Abstract

Statistical Energy Analysis (SEA) is a powerful tool to describe energy sharing in a complex structure. To apply this method, the structure must be divided into subsystems. One of the main drawback of this method is the difficulty in finding subsystems which verify SEA assumptions. Moreover, the weak coupling between subsystems is not well defined despite it being one of the most important assumptions of SEA. This paper deals with the derivation of a tool to aid decision-making in SEA substructuring. It is based on a cluster analysis to classify energy transfer functions and on principal component analysis (PCA) to reduce data size. The method is applied to three test cases: an L-shaped plate, an assembly of three plates and a complex thin shell structure.

1. Introduction

Statistical Energy Analysis (SEA) was first introduced by Lyon and Maidanik [1] and Smith [2] in the early 1960s. The power flow between two independently and randomly excited harmonic oscillators was calculated assuming a linear coupling. An equation linking power flow and energy of the subsystems was established. Then the model was extended to the problem where two multimodal systems interact.

One of the main difficulties in applying SEA to complex industrial structures is the lack of methodology in substructuring. Indeed, as Langley [3] defined it, an SEA model has to be divided

*Corresponding author. Tel.: +33 172436392.
E-mail address: nicolas.totaro@lva.insa-lyon.fr (N. Totaro).

0022-460X/$ - see front matter © 2005 Elsevier Ltd. All rights reserved.
doi:10.1016/j.jsv.2005.03.030

into reverberant subsystems connected by a weak coupling. Subsystems are usually defined as groups of modes or wave types having approximately the same energy. The impedance mismatch between subsystems has to be high enough so that mode shapes of uncoupled subsystems are not modified by the coupling. Subsystems must have a moderate damping: high enough to have an impedance mismatch between subsystems, but low enough to have a reverberant subsystem.

Several papers deal with the derivation of coupling loss factors (CLFs) in order to estimate the coupling strength between two subsystems. Mace [4] has introduced four distinct strengths of coupling and two coupling parameters which govern the transition between them. The coupling is defined by reflection and transmission coefficients and coupling parameters depend on transmission coefficient and on subsystems modal overlaps. Finnveden [5] has studied ensemble-averaged vibration energy flows in a three-element structure and found a coupling parameter close to Mace's. He showed that the SEA hypothesis is true if the coupling is weak between two reverberant subsystems. Langley [3] has given a definition of weak coupling based on Green's functions: the coupling will be said to be weak if there exists a small parameter ε such that the Green function $|G_{ij}(x,y,\omega)|^2$ is of order $o(\varepsilon^n)$, where n represents the minimum number of couplings which separate subsystem i from subsystem j.

Maxit and Guyader [6,7] have presented an approach based on the use of the dual modal formulation (DMF) applied to two coupled subsystems to determine the modal coupling coefficients. In the case of complex subsystems, FEM can be used to deduce the CLFs.

Experimental determination of CLF have also been developed. For example, Bies and Hamid [8] determined loss and CLFs of coupled plates. The inversion of SEA equations was used as basic method (the power injected method, PIM) to identify CLF from measured energies. Fahy, James and Price [9,10] have shown that, when one subsystem is subject to impulsive excitation, the time delay in the rise of the kinetic energy in the indirectly excited subsystem can be used as an indicator of coupling strength.

All these works suppose the a priori knowledge of subsystems. But the identification of subsystems is not obvious in complex industrial cases. The present paper deals with a method to determine the number and the location of subsystems of a complex structure. This method is based on cluster analysis, that is a classification tool used to find groups in a database [11,12]. K-means algorithm [12] classifies a database of N vectors described by M variables in K groups or clusters. Finally, two data points contained in the same group are more similar than two data points contained in two different groups. Dissimilarity between two data points is measured by their Euclidean distance. This method is applied to three different cases: a classical L-shaped plate, an assembly of three plates and a complex thin shell structure.

2. Kinetic and strain energies

As SEA deals with energy sharing, it seems relevant to use energy transfer function in order to detect points having the same behavior and thus belonging to the same subsystem. For numerical simulation, kinetic and strain energy can be calculated but, in experimental SEA, only kinetic energy can be measured. The energy balance is correct in both cases and, generally, one assumes equality of strain and kinetic energies. This is probably true for the global energy of an isolated subsystem excited by white noise, but there is no evidence of this when subsystems energies are

considered and even more for energy density (ratio between energy of an element and its surface or volume). Experimental methods to estimate CLF like Power Injection Method (PIM) assume that kinetic energy correctly represents energy sharing between subsystems, but if this assumption is not verified the results cannot be correct. Inversely, SEA predictions cannot be verified experimentally, even if CLF are exact, if subsystems energies are not well estimated.

As we want, in the present approach, to compare the behaviors of each element of the structure to find subsystems, it is relevant to use a local quantity. Thus, it is important to verify if kinetic energy is sufficient to correctly describe the energy flow between elements or if it is necessary to compute total energy.

Some numerical simulations have been carried out to evaluate the kinetic and strain energies in a system excited by a point force. When a finite element is used, kinetic and strain energies of element e_i can be defined as

$$E_k^{e_i}(\omega) = \tfrac{1}{2}\omega^2 \mathbf{W}_{e_i}^{\mathrm{T}} \mathbf{M}_{e_i} \mathbf{W}_{e_i}, \tag{1}$$

$$E_s^{e_i}(\omega) = \tfrac{1}{2} \mathbf{W}_{e_i}^{\mathrm{T}} \mathbf{K}_{e_i} \mathbf{W}_{e_i}, \tag{2}$$

where $\mathbf{W}_{e_i}$ is the nodal displacement vector of element e_i and $\mathbf{M}_{e_i}$ and $\mathbf{K}_{e_i}$ are, respectively, the mass and stiffness matrices associated to element e_i. In the following, the energy densities per element will be taken into account. The kinetic and strain energy densities per element is calculated dividing contribution of each element by its associated area in order to have a quantity independent of mesh size

$$\bar{E}_k^{e_i}(\omega) = E_k^{e_i}(\omega)/S^{e_i}, \tag{3}$$

$$\bar{E}_s^{e_i}(\omega) = E_s^{e_i}(\omega)/S^{e_i}, \tag{4}$$

where S_{e_i} is the area of element e_i. $\langle \bar{E}_s^{e_i}(\omega) \rangle$ will denote the frequency-averaged kinetic energy density. In addition, the kinetic and strain energies of the system can be obtained by summing contribution of each element over the whole system

$$E_k(\omega) = \sum_{i=1}^{N_e} E_k^{e_i}(\omega), \tag{5}$$

$$E_s(\omega) = \sum_{i=1}^{N_e} E_s^{e_i}(\omega). \tag{6}$$

Let us take two examples to compare kinetic and strain energies. The first one is a simply supported thin plate excited by a point force. Fig. 1 shows the kinetic and strain energies of the plate for 500 Hz octave band. In this case, the global kinetic energy $E_k(\omega)$ is almost equal to the global strain energy $E_s(\omega)$.

One can see on Fig. 2 that differences between frequency-averaged kinetic and strain energy densities ($\langle \bar{E}_k^{e_i}(\omega) \rangle$ and $\langle \bar{E}_s^{e_i}(\omega) \rangle$) can become significant especially near boundaries.

For a complex thin shell structure, the equality of strain and kinetic energy densities is almost achieved in flat areas (A-zone, Fig. 3). Nevertheless, in curved zones (B-zone), the frequency-averaged strain energy density is higher than the frequency-averaged kinetic energy density. The

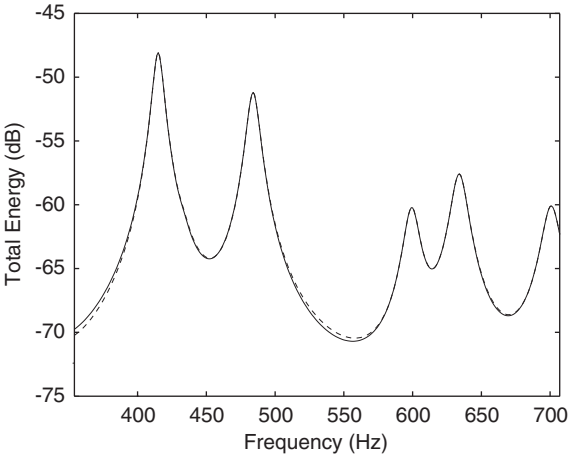

Fig. 1. Comparison between kinetic and strain energies of a simply supported plate ($a = b = 1$ m, $h = 10$ mm). 500 Hz octave band.

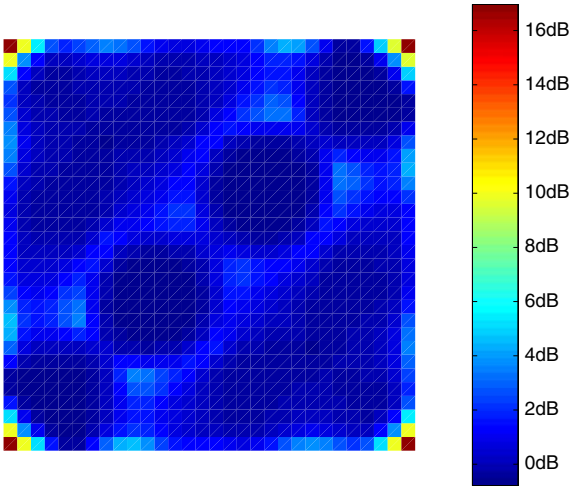

Fig. 2. Differences between $\langle \tilde{E}_s^{e_i}(\omega) \rangle$ and $\langle \tilde{E}_k^{e_i}(\omega) \rangle$ of a simply supported plate ($a = b = 1$ m, $h = 10$ mm). Frequency averaged over 500 Hz octave band.

opposite situation appears in high velocity zones (C-zone). Industrial structures are often more complex than this test case, including structural heterogeneities for example. Thus, in the present approach, it is important to estimate both kinetic and strain energies in order to correctly describe energy sharing through the structures.

However, differences between frequency-averaged kinetic and strain energy densities decreases with frequency (see Fig. 3), even if, up to 1000 Hz, it still remains significant (especially in the B-zone). Using only the kinetic or strain energy densities can give, at low frequency, a wrong description of the energy sharing in a complex structure. Thus, the total energy density (sum of kinetic and strain energy densities) will be used in the following.

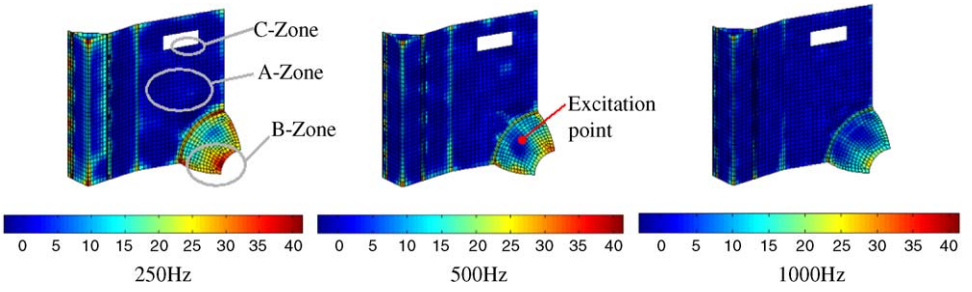

Fig. 3. Differences between $\langle \bar{E}_s^{e_i}(\omega) \rangle$ and $\langle \bar{E}_k^{e_i}(\omega) \rangle$ of the complex test case. Frequency averaged over 250, 500 and 1000 Hz octave bands.

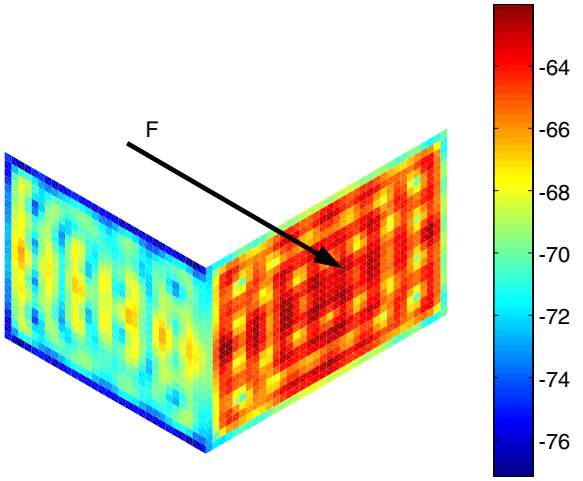

Fig. 4. Total energy density in dB (ref = 1). Frequency averaged over 500 Hz octave band.

2.1. Principal components decomposition of the energy transfer functions

To find subsystems, a database composed by energy transfer functions will be classified into groups of elements having the same behavior when the structure is excited by different point forces. To compare and classify energy transfer functions, some parameters describing them must be used. Regarding this, the principal components analysis (PCA) is a powerful tool to find automatically independent parameters which describe a database. Then, each transfer function is projected on the first N_P principal components. One obtains N_P parameters sorted in importance order and transfer functions can be classified by comparing their associated parameters (called PCP parameters: Principal Component Projection). In the following, each database is represented by the associated PCP matrix. Such a method was applied by Zang et al. [13] to detect default into a railway wheel.

Let us take the example of an L-shaped plate presented in Fig. 4. This structure, modeled by 1544 finite elements, is excited by a point pure tone force. In order to have a frequency description

of the energy densities in the octave band centered at 500 Hz, calculations were made at 234 frequencies in the octave band. The frequency-averaged total energy densities are presented in Fig. 4. The energy transfer matrix is then composed of 1544 columns of transfer functions and 234 frequency lines. The following procedure is then applied.

2.1.1. One excitation point

The matrix $\mathbf{E}$ (with N rows and M columns) composed by N energy transfer functions and M frequency lines is considered. The component positioned row i and column j is denoted e_{ij}. A PCA of this matrix will be applied. In the following, the PCA will correspond to the projection of the normalized matrix $\tilde{\mathbf{E}}$ in the space of eigenvectors of a square correlation matrix $\mathbf{C}$ defined as the product $\tilde{\mathbf{E}}^{\mathrm{T}}\tilde{\mathbf{E}}$.

The mean value of the jth column (resp., the standard deviation) is defined, respectively, as below,

$$\bar{E}_j = \frac{1}{N}\sum_{i=1}^{N} e_{ij}, \tag{7}$$

$$S_j^2 = \frac{1}{N}\sum_{i=1}^{N} (e_{ij} - \bar{E}_j)^2. \tag{8}$$

Each element e_{ij} of the matrix $\mathbf{E}$ can be normalized as expressed in Eq. (9) and becomes a variation matrix $\tilde{\mathbf{E}}$

$$\tilde{e}_{ij} = \frac{e_{ij} - \bar{E}_j}{S_j\sqrt{N}}. \tag{9}$$

The correlation matrix is then defined as

$$\mathbf{C}_{M\times M} = \tilde{\mathbf{E}}^{\mathrm{T}}_{M\times N}\tilde{\mathbf{E}}_{M\times N}. \tag{10}$$

The eigenvectors and eigenvalues are finally calculated and sorted in a descending order. A couple composed by an eigenvalue λ_i and its associated eigenvector $\mathbf{\Psi}_i$ is called principal component. One has

$$\mathbf{C}\mathbf{\Psi}_i = \lambda_i\mathbf{\Psi}_i. \tag{11}$$

The most important principal component is the first one, it indicates the direction having the maximum variability in the database. Then the normalized matrix $[\tilde{\mathbf{E}}]$ can be projected on the P first eigenvectors

$$\mathbf{PCP}_{N\times P} = \tilde{\mathbf{E}}_{N\times P}\mathbf{\Psi}_{P\times P}. \tag{12}$$

Using PCA, each transfer function of the matrix can be described by the first N_P PCP parameters.

Fig. 5 presents three energy transfer functions (ETF_1, ETF_2 and ETF_3) extracted from the transfer matrix and theirs associated PCP parameters.

As one can see on Fig. 5(a), the energy transfer functions ETF_1 and ETF_2 have close behaviors whereas ETF_3 is very different. These differences can be also observed on the associated PCP parameters. Indeed, Fig. 5(b) shows that PCP of ETF_1 and ETF_2 are almost equivalent whereas

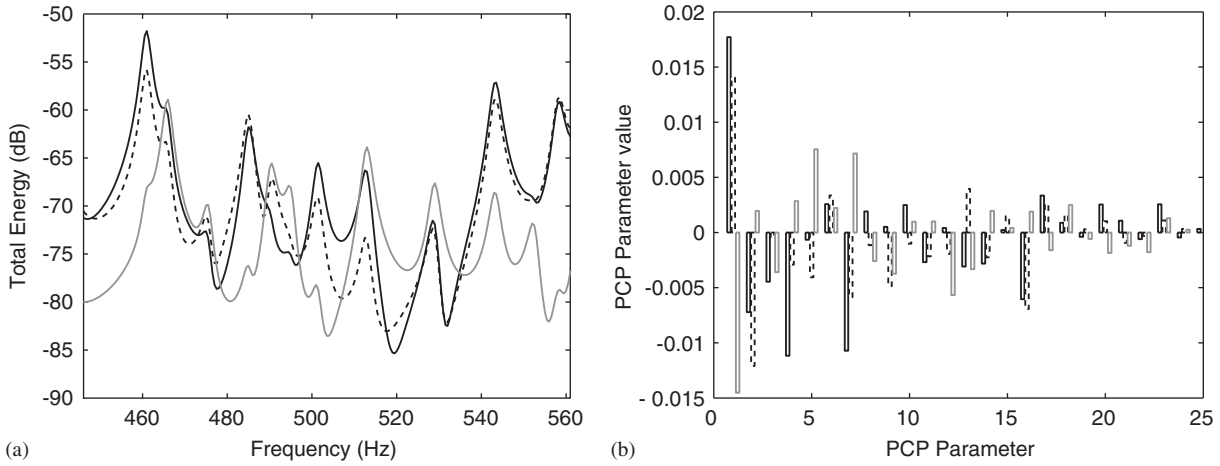

Fig. 5. Example of energy transfer functions (a) and their principal component decompositions (representation of the 25 PCP parameter values for each transfer functions) (b) - -: energy transfer function ETF_1; — black: ETF_2; — gray: ETF_3.

they differ from ETF_3 on PCP parameters number 1, 2, 5 and 7. Thus, it is possible to classify energy transfer functions by comparing their associated PCP parameters.

2.1.2. Several excitation points

The structure is excited by several different uncorrelated point forces. For each excitation point, a PCP is carried out and a PCP matrix is obtained. The global database is constructed assembling matrices $\mathbf{PCP}_{N\times P}$ obtained for each excitation i

$$\mathbf{D}_{N\times(P_1+P_2+\cdots+P_n)} = [\mathbf{PCP}^1_{N\times P_1}\mathbf{PCP}^2_{N\times P_2}\ldots\mathbf{PCP}^n_{N\times P_n}]. \tag{13}$$

In SEA, modal energy is used rather than energy density. However, the estimation of number of modes in a frequency band for each group of elements is quite difficult with global modes and the modal energy per subsystems cannot be obtained easily. The PCP permits to describe energy transfer functions by parameters. It has been demonstrated [14] that the first PCP parameter is proportional to the difference $\langle\bar{E}_t^{e_i}(\omega)\rangle - \langle\bar{E}_t(\omega)\rangle$ (difference between energy on an element and energy of the structure). Other PCP parameters are more difficult to interpret but the number and the position of picks in the frequency band are necessarily described by PCP parameters. On account of these remarks, it has been chosen to do substructuring with energy density transfer functions rather than with an estimation of modal energy per group of elements.

The energy transfer matrix (size 1344×234) is replaced by the PCP matrix (size 1344×25) to classify the different elements of the structure. Taking into account only the 25 first principal components does not lead to a significant loss of information because they represent 99% of the variability of the database. This is a considerable reduction of the size of the database without a real loss of information. Moreover, the reduction can be more drastic. In order to simply understand the substructuring technique, only the two first PCP parameters will be used in the following. Obviously, in real application the method has to be applied with more PCP parameters. Fig. 6 shows the first PCP parameter of the energy transfer database as a function of the second

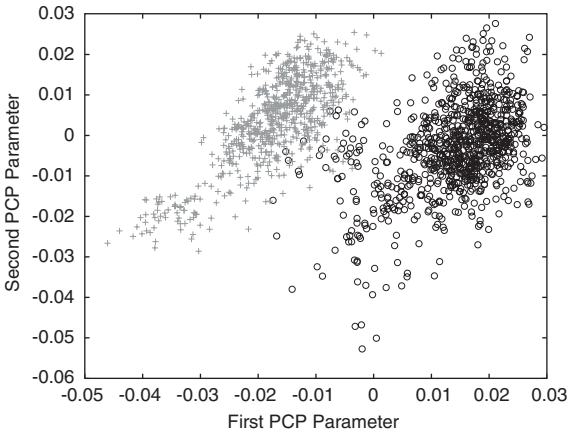

Fig. 6. First PCP parameter as a function of the second one for every transfer functions of the database. gray +: measuring points located on plate 1; black ○: measuring points located on plate 2 (Table 1).

one. As one can see on Fig. 6, even if the reduction of information is extreme, it is easy to differentiate the two plates.

2.2. *Cluster analysis: A classifying tool*

A lot of algorithms exist to classify a set of data into groups having almost the same behavior. Despite its simplicity, *k*-means algorithm is one of the most commonly used in cluster analysis [15]. Its basic concept is very easy to understand but, for sake of simplicity, the process will be illustrated using only the two first principal component of the decomposition (Fig. 6). Obviously, cluster analysis could be done in a *N*-dimensional space.

Cluster analysis is the process of partitioning a database of N points represented by P parameters into K groups or clusters. Each cluster is represented by its mass center. The *k*-means algorithm is in three steps

Step 1: An initial partition is done, that is to say that K data points are chosen to be the mass centers of clusters. Many different methods could be used to choose initial mass centers and a comparison of them is described in Ref. [16]. In the following, mass centers will be chosen randomly (Fig. 7(a)).

Step 2: Each point is assigned to the cluster whose mass centers is nearest (Fig. 7(b) for the first iteration).

Step 3: Position of the mass centers is then updated (Fig. 7(c) for the first iteration). This is simply done by averaging positions of each points of the cluster along each dimension.

The second and third steps are repeated while the positions of mass centers are not stabilized (Figs. 7(c)–(f)).

When the classification is done, it is easy to visualize groups of points of the plate belonging to a cluster. The substructuring of the L-shaped plate is presented in Fig. 8.

One has to bear in mind that this substructuring has been done with a particular initial partition and with only two parameters describing transfer functions.

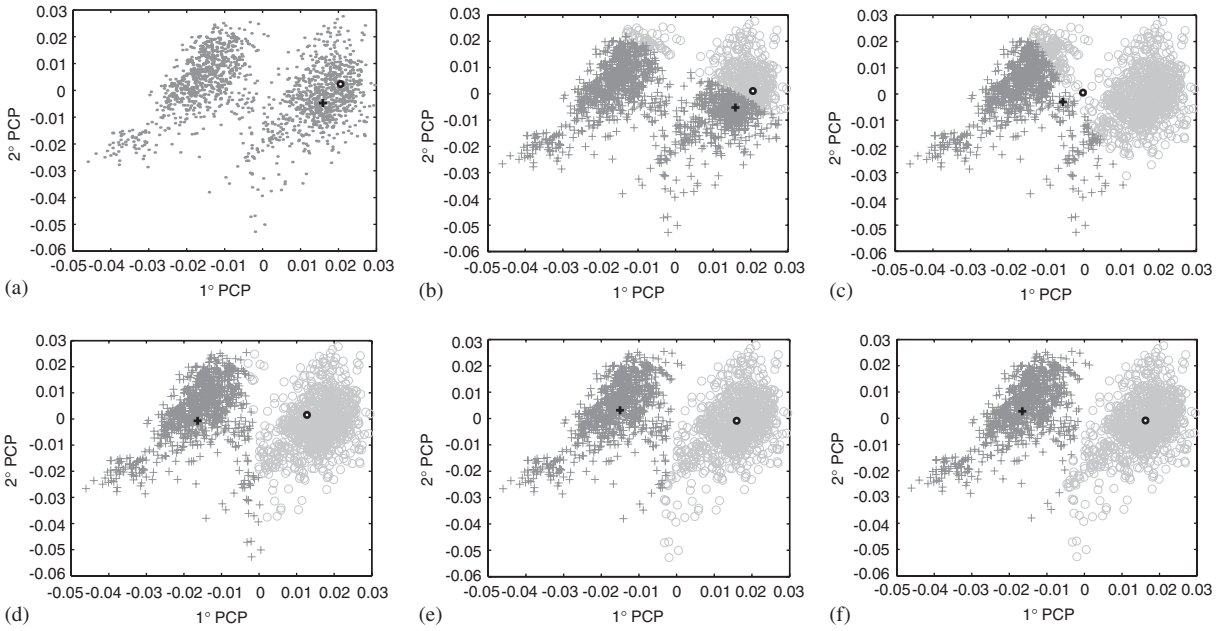

Fig. 7. Evolution of the partition of the database for four iterations. black + and ○: gravity centers of groups 1 (+) and 2 (○); gray + and ○: PCP vectors associated to groups 1 (+) and 2 (○). (a): initial positions of gravity centers; (b): initial partition; (c): first iteration of cluster analysis; (d): second iteration; (e): third iteration; (f): fourth iteration, final partition.

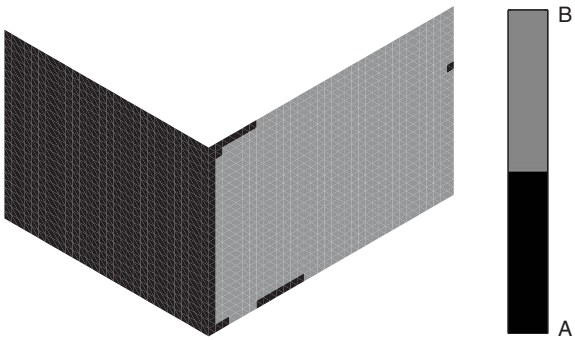

Fig. 8. Substructuring of the L-shaped plate for 500 Hz octave band.

Substructuring depends on initial position of mass centers and could be slightly modified according to them. In order to overcome this drawback, several substructuring have been done for different initial partitions. The one which minimize the validity index $\mathscr{M}$ is taken as the optimal one. Index $\mathscr{M}$ is given by (see Ref. [17])

$$\mathscr{M} = \sum_{j=1}^{K} \sum_{x_i \in C_j} \|x_i - X_j\|, \tag{14}$$

where K is the number of clusters, x_i are the coordinates of point i and X_j are the coordinates of mass center j.

3. Best number of subsystems

3.1. A weak coupling criterion: The γ criterion

The substructuring of an L-shaped plate is obvious and the a priori number of subsystems is known. But, in the major part of applications it is not the case. Thus, the cluster analysis should be done with different number of clusters and an index should be developed in order to find the optimal number of subsystems of a given structure. Standard case of a L-shaped plate is considered as a validation case because it has been intensively studied and a lot of data are available. In particular, Mace [4], Mace and Rosenberg [18] and Finnveden [5] have defined a coupling parameter γ which can be used to give an estimate of the coupling strength between two edge coupled plates. This criterion is given by

$$\gamma = \frac{\tau_{ij}}{\pi^2 M_i M_j}, \tag{15}$$

where $M_i = \eta_i \omega n_i(\omega)$, η_i is the damping loss factor and $n_i(\omega)$ is the modal density of plate i and τ_{ij} is the transmission coefficient.

For the assembly of two plates, the coupling parameter γ is a function of frequency and damping coefficient as it is shown Fig. 9 for the plates described in Table 1.

The coupling between the two plates is considered to be weak if $\gamma < 1$. Thus, for a given frequency, it exists a limit of damping under which coupling is too strong to consider the two plates as different SEA subsystems. Two cases are taken into account in the following:

- strong coupling case for 500 Hz octave band and damping coefficient equal to 0.5%,
- weak coupling case for 500 Hz octave band and damping coefficient equal to 3%.

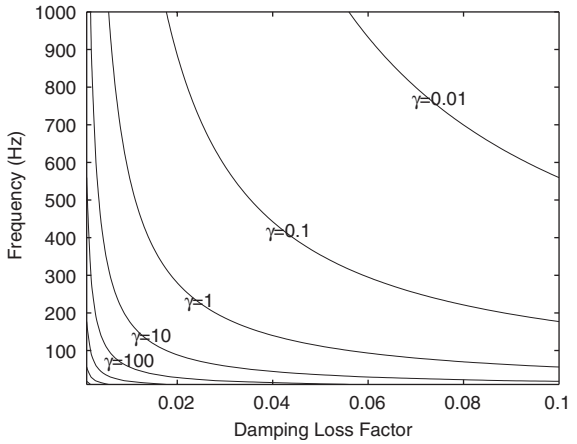

Fig. 9. Coupling parameter γ as a function of frequency and damping coefficient for the assembly described in Table 1.

Table 1
Characteristics of the plates of the L-shaped assembly

	Plate 1	Plate 2
Length (m)	0.8	0.6
Width (m)	0.8	0.8
Thickness (mm)	1	1
Material	Steel	Steel

Applying a substructuring method, one must find two subsystems in the case of weak coupling and only one subsystem in the case of strong coupling. Thus, optimal number of subsystems can vary with frequency or damping. Even for such a simple case, it is finally difficult to a priori know the number of subsystems.

In cluster analysis, the number of subsystems is used as an input. To overcome this difficulty, one can propose to divide the system into an increasing number of subsystems and find a posteriori the optimal number of subsystems as it is done in Refs. [19–21]. The substructuring which minimizes a validity index will be taken as the best one.

3.2. *The* mir(i,j) *index: A validity index*

The Mutual Inertia Ratio (mir) given in Eq. (17) is a measure of dissimilarity between two subsystems. It is defined as the ratio of intra-cluster and inter-clusters inertia of two groups of points of a given partition

$$\mathrm{mir}(i,j) = \frac{I^i_{\mathrm{intra}} + I^j_{\mathrm{intra}}}{I^{ij}_{\mathrm{inter}}} = \frac{\sum_{x_n \in C_i} d(x_n, g_i) + \sum_{x_m \in C_j} d(x_m, g_j)}{N_i\, d(g_i, g_{ij}) + N_j\, d(g_j, g_{ij})}, \tag{16}$$

where N_i is the number of elements in cluster i, $d(x_n, g_i)$ is the euclidean distance between point x_n and mass center of cluster i, $d(g_i, g_{ij})$ is the euclidean distance between mass center of cluster i and mass center of the union of cluster i and cluster j.

MIR index is defined as maximum value of the mir(i,j) index.

$$\mathrm{MIR} = \max(\mathrm{mir}(i,j)). \tag{17}$$

The substructuring of a given assembly of plate (see Table 1) into two subsystems is investigated for different frequency band, different damping and different position of excitation. Each time, mir$(1,2)$ between plates is calculated. Fig. 10 represents MIR as a function of the γ criterion.

According to γ criterion, two zones can be defined. Above $\gamma = 1$, the coupling is strong and both plates belong to the same subsystem. Below $\gamma = 1$, coupling is weak and each plate is a subsystem. Thus, the mir(i,j) scale index can be divided into three zones.

- γ criterion is equal to one (weak coupling limit) for a MIR value ranging between 1.3 and 2,
- above mir$(i,j) = 2$, γ criterion is always higher than 1,
- below mir$(i,j) = 1.3$, γ criterion is always lower than 1.

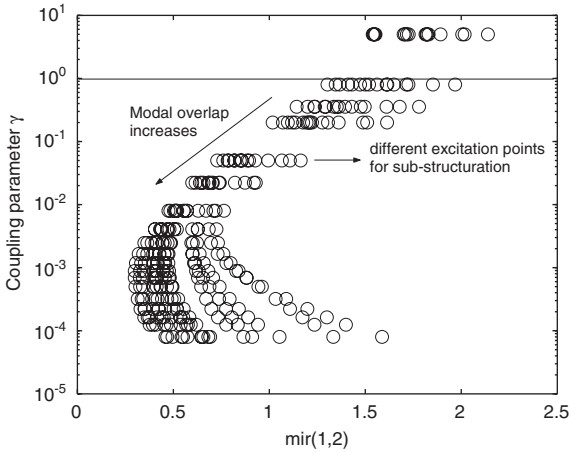

Fig. 10. Mutual Inertia Ratio as a function of Mace's criterion. Each point is obtained during the sub-structuring of assembly described by Table 1 at different frequency bands and for different structural dampings and with different excitation points.

Thus, one can deduce that mir(i,j) can be used as an indicator of classification validity in terms of SEA substructuring

- if mir$(i,j)<1.3$ for a couple of subsystems, one can say that these subsystems *are* dissimilar enough to be considered as two different SEA subsystems,
- if mir$(i,j)>2$ for a couple of subsystems, one can say that these subsystems *are not* dissimilar enough to be considered as two different SEA subsystems,
- if $1.3<$mir$(i,j)<2$ for a couple of subsystems, the decision is not clear.

One can see that, for high modal overlap, mir(i,j) increases and can be higher than 1.3 even if Mace's criterion is still lower than 1. When modal overlap is so high, the subsystem is not reverberant any more and its energy is not constant on its whole surface. In that case, the assumption of reverberant subsystems is not verified and SEA gives bad results. Heron [22] shows that SEA over-estimates power flow around a plate or beam network for high frequency. For an assembly of six rods, SEA is shown to over-estimate exact results up to 60 dB. Thus, it seems to be appropriate to have two limits of validity for SEA: one for low modal overlap (Mace's criterion) and another one for very high modal overlap. mir(i,j) behavior agrees with such limits. mir(i,j) can also be used as an indicator to find the best number of subsystems. In effect, if the highest mir(i,j) value (MIR index) is lower than the weak coupling limit defined with the γ criterion, then subsystems have dissimilar enough behaviors to be considered as SEA subsystems. The number of subsystems which minimize MIR index can be taken as the best one found by the algorithm.

Whereas γ criterion is only suitable to simple structures like assemblies of plates, MIR index does not depend on the complexity of the subsystems and can be applied to any structures. On the other hand, it is only an indication on the best substructuring with respect to other proposed partitions. This index is based on mathematical considerations and extends results observed with γ criterion on L-shaped assemblies to more complex structures. It is here supposed that MIR index

calibrated on simple cases can be used as a useful measure of SEA validity for any kind of structure. This empirical assumption has to be validated: the following parametric study of mir(i,j) index tries to demonstrate that mir(i,j) index is a good indicator of behavior dissimilarity between subsystems and can be correlated to coupling strength between subsystems.

4. Parametric study of the mir(i,j) index

To better understand behavior of the mir(i,j) index (Mutual Inertias Ratio between subsystems i and j) a parametric study of academic assemblies of plates will be done. Assemblies of rectangular plates are often taken as reference case in SEA. However, even if these structures are some of the most simple to apply SEA, they are driven by several parameters like coupling angle, thickness ratio between plates or frequency. An usually accepted expression of CLFs between two subsystems, detailed by Wöhle et al. [23], is given by

$$\eta_{12} = \frac{c_{g_1} L}{\pi \omega S_1} \bar{\tau}_{12}, \tag{18}$$

where c_{g_1} is the group velocity of bending wave of plate 1, L is the coupling length, S_1 is the area of plate 1 and $\bar{\tau}_{12}$ is the averaged transmission coefficient between plates 1 and 2. The evaluation of the transmission coefficient is not easy because it depends on assembly (coupling angle) and plates (thickness) characteristics. As for γ criterion, it is difficult to apply formula (18) for assemblies of non-rectangular subsystems.

4.1. *Evolution of the* mir(i,j) *index as a function of coupling angle between two plates*

Fig. 11(a) presents the sketch of the assembly used to study influence of coupling angle θ on mir(1, 2) index.

Rebillard [24] and Ouisse and Guyader [25] established that the coupling angle is a parameter which can considerably modify behavior of an assembly of plates especially for small angles.

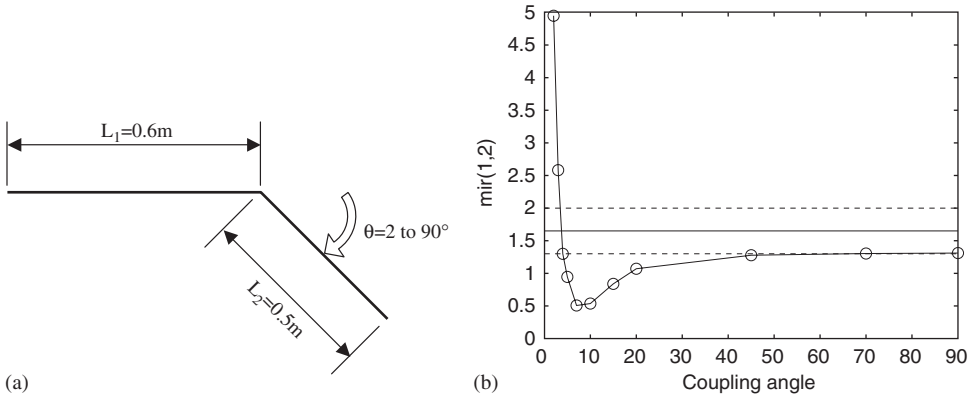

Fig. 11. (a) Sketch of the assembly (two plates made of steel, width 0.4 m) and (b) evolution of the mir(1, 2) index as a function of coupling angle for 1000 Hz third octave band.

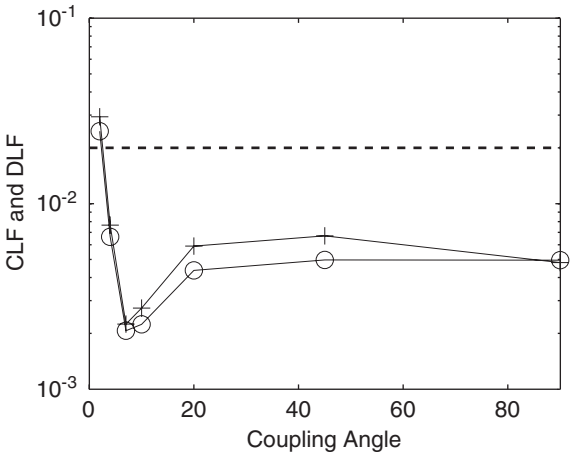

Fig. 12. Evolution of coupling loss factor as a function of coupling angle between plates described in Fig. 11(a) for 1000 Hz third octave band (damping: 2%). –○–: CLF_{12}; –+–: CLF_{21}. CLF are calculated using Energy Influence Coefficients and inverse SEA.

Analysis of the mir(i,j) index allow us to evaluate the coupling strength between plates. Fig. 11 demonstrates that the coupling strength vary with the coupling angle. mir$(1,2)$ is almost constant for angles ranging between 90° and 20°. Below 20°, mir$(1,2)$ decreases and reaches a minimum for an angle of 7°. Below 7°, mir$(1,2)$ quickly increases and shows that coupling strength between plates becomes stronger and stronger. Thus, for 1000 Hz third octave, this assembly can be divided into two subsystems for angles upper than 4°, but must be considered as one SEA subsystem for angles smaller than 4°.

These remarks are confirmed by calculating CLF between plates. The CLF are calculated using the Energy Influence Coefficients introduced by Guyader et al. [26] to evaluate the subsystems energies when one is excited by a δ-correlated force. An energy matrix is build to apply inverse SEA and deduce CLFs. Fig. 12 presents evolution of CLFs η_{12} and η_{21} as a function of the coupling angle (1000 Hz third octave band, damping: 2%). It confirms that CLFs between plates follows the same tendencies as mir$(1,2)$ index. CLFs are almost constant for angle ranging between 90° and 20°, are minimum for angles close to 7° and highly increase for very small angles.

The present approach, using total energy, does not differentiate in-plane and out-of-plane motions, and thus, it cannot find two different subsystems in the same substructure (an in-plane subsystem and an out-of-plane subsystem on the same plate for example). It would be possible to differentiate these motions by calculate in-plane and out-of-plane energies. However, complex curved structures have in-plane and out-of-plane motions totally coupled and such phenomenon is restricted to flat plates.

4.2. *Evolution of the* mir(i,j) *index as a function of thickness ratio between two plates*

Let us take the example of two coupled plates of different thicknesses, described in Fig. 13(a). The thickness ratio between plate 1 (fixed thickness: 1 mm) and plate 2 varies between 2 and 10. Fig. 13(b) presents the evolution of mir$(1,2)$ as a function of the thickness ratio.

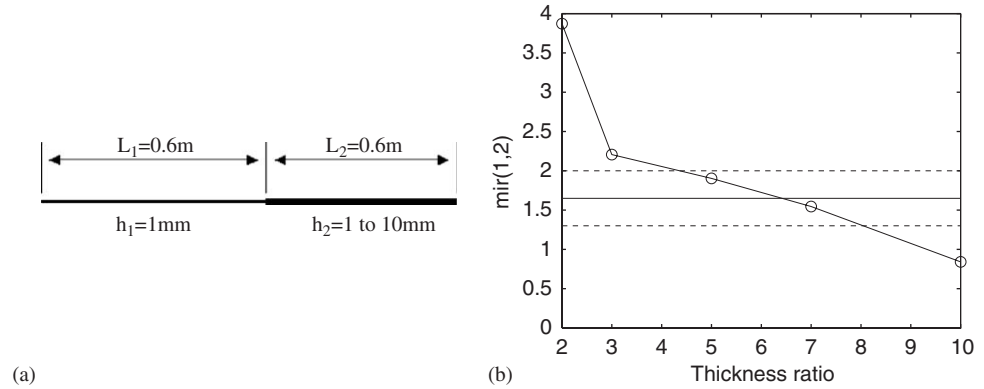

Fig. 13. (a) Sketch of the assembly (two plates made of steel, width 0.4 m, thickness 1 mm, damping 2%) and (b) evolution of the mir(i,j) index as a function of thickness ratio for 1000 Hz third octave.

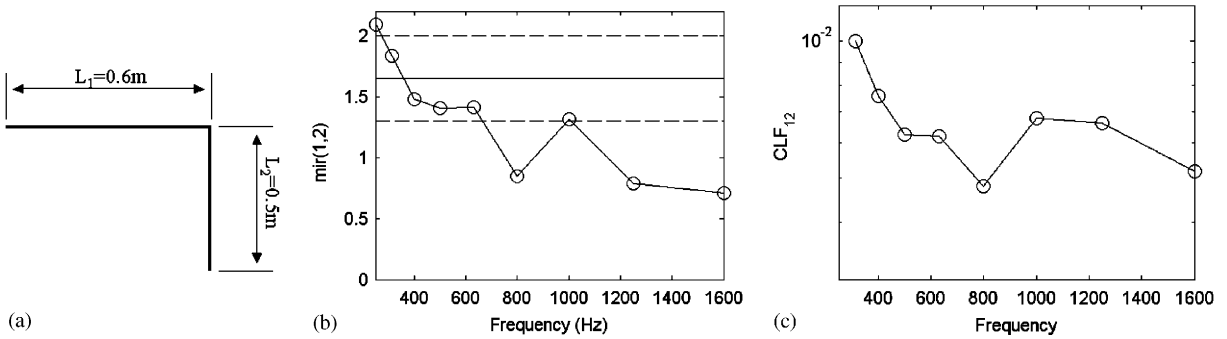

Fig. 14. (a) Sketch of the assembly (two plates made of steel, width 0.4 m, damping: 2%); (b) evolution of mir(1, 2) index versus frequency and (c) evolution of coupling loss factor versus frequency, CLF are calculated using Energy Influence Coefficients and inverse SEA.

The mir(1, 2) index is almost proportional to thickness ratio between plates. The mir(1, 2) index criterion indicates that the assembly can be divided into two subsystems for thickness ratio upper than 5 or 6.

4.3. *Evolution of the* mir(i,j) *index as a function of frequency*

It is obvious that coupling strength depends on frequency band as predicted by γ criterion. mir(1, 2) index of L-shaped coupled plates (Fig. 14) is calculated for 250 to 1600 Hz third octave bands. The evolution of the mir(1, 2) index as a function of frequency is presented in Fig. 14.

Fig. 14(b) shows that mir(1, 2) tends to decrease with frequency and this is of course an expected result demonstrating that an assembly of plate must be modeled as one or two SEA subsystems depending on the frequency band. Fig. 14(c) presents evolution of CLF between plates versus frequency. Correlation between CLF and mir(1, 2) is clear. mir(1, 2) is a good indicator of

coupling strength between plates. It is then possible to define if a substructuring is valid for SEA analyzing mir(i,j) and MIR indices.

4.4. *Evolution of the* mir(i,j) *index as a function of coupling type*

In this example, a finite element model is used to calculate response of coupled plates. Four types of coupling having different stiffnesses will be studied. Coupling types are detailed in Fig. 15. In the first case, the plates are connected at all nodes of the coupling line. In the second and third cases, the two plates are connected by twelve welded points modeled respectively by

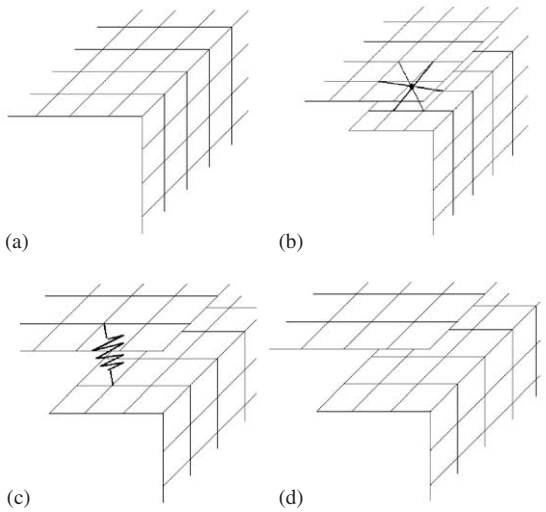

Fig. 15. Coupling line between plates: (a) plates connected at all nodes of the coupling line (fully connected); (b) welded point modeled by RBE2 elements; (c) welded point modeled by CELAS2 elements and (d) plates not coupled.

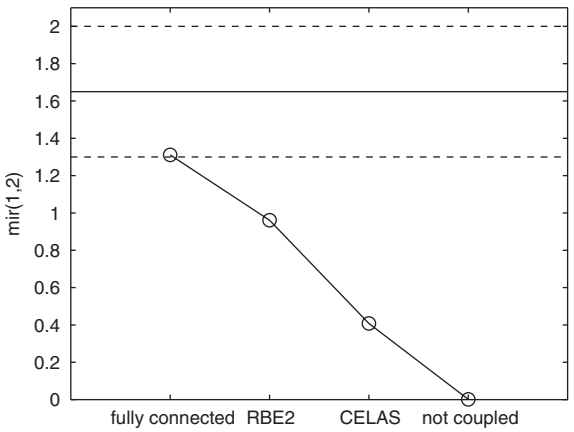

Fig. 16. Evolution of mir(1, 2) index as a function of coupling types described in Fig. 15 for 1000 Hz third octave band.

RBE2 (rigid elements) and CELAS2 (springs) elements (torsional stiffness: $1e9\,\mathrm{N\,m\,rad^{-1}}$, translational stiffness: $1e6\,\mathrm{N\,m^{-1}}$). In the fourth case, plates are not coupled.

Fig. 16 presents the mir(1, 2) index in these four cases. The mir(1, 2) index clearly decreases with coupling strength. Moreover, when the plates are not coupled, it tends to a value close to zero as CLFs.

5. Number of excitation points

In this section, stability of the method necessary to obtain a good substructuring is studied and lead to a minimal number of excitations points. A simple assembly of three plates is taken as example (see Fig. 17).

It is necessary to excite complex structures at several different points in order to detect all the possible subsystems. Indeed, two different subsystems can react in the same manner for a given excitation and have different behaviors with another excitation point. Principal component decomposition of energy transfer functions is carried out for each excitation. The N_{exc} PCP matrices obtained are gathered into a single matrix which will be used for classification.

The substructuring is done using an increasing number of excitations (1–6, see Fig. 17). The mir(i, j) between subsystems is calculated each time. Damping coefficient is set to 3% in order to have weak coupling between each plate according to γ criterion. In this case, obviously, the method is expected to find three subsystems. Fig. 18 represents results of classification using one to six excitations.

It can be seen that, with only one excitation point it is impossible to correctly differentiate non-excited plates. On the other hand, only two excitations are sufficient to differentiate the three plates. In addition, the substructuring is stable with the increase in the number of excitations. It can be seen in Fig. 18 that for two to six excitations, MIR index always indicates that the structure should be divided into three subsystems.

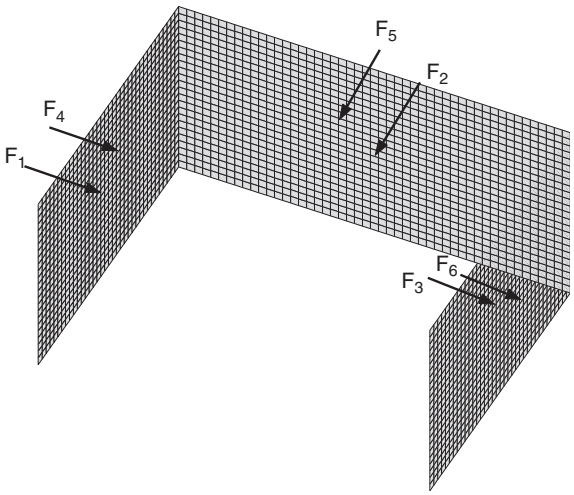

Fig. 17. Mesh of the assembly of three plates and location of excitation points.

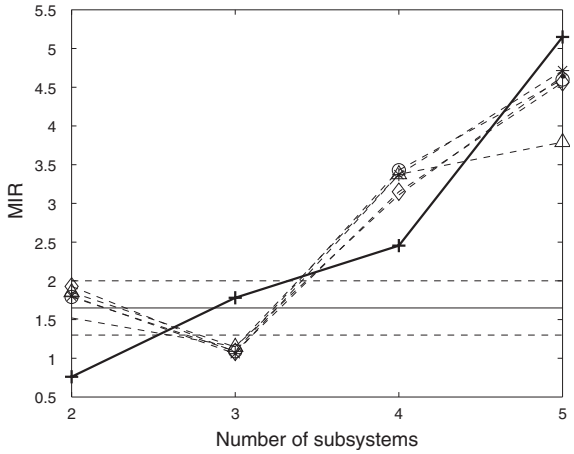

Fig. 18. MIR index as a function of number of subsystems for different numbers of excitations.

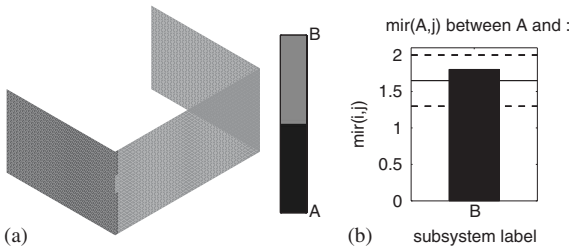

Fig. 19. (a) Substructuring of the three plates structure into 2 subsystems; (b) mir(i,j) indices between subsystems A and B. 500 Hz third octave band, damping: 3%.

Consequently, extending this result to an assembly of X subsystems, one can expect that only $X-1$ excitations are sufficient for a good substructuring but a larger number of excitations is possible. The best number of excitation points is obtained when MIR index does not vary any more even if the number of excitations is increased.

Let us take the case of three excitations (one excitation on each plate). The analysis of MIR index indicates that best number of subsystems is three, however it is interesting to see to what kind of substructures the method leads when two, four and five subsystems are considered even if they cannot be used as SEA subsystems. Figs. 19–21 present the system substructured into two, three and four subsystems and some associated mir(i,j) values.

- In the case of two subsystems (Fig. 19(a)), one plate is taken as a subsystem and the two others are gathered into the second subsystem. As the value of MIR index is slightly higher than validity limit, this substructuring seems not to be suitable for an SEA application.
- In the case of three subsystems (Fig. 20(a)), each plate is found to be a subsystem as it could be predicted using γ criterion (Eq. (15)). The MIR index indicates that this substructuring can be used for SEA applications. mir(B,A) and mir(B,C) are almost equal due to symmetry. One can also see that, mir(A,C) is not zero even if these subsystems are not physically connected. The

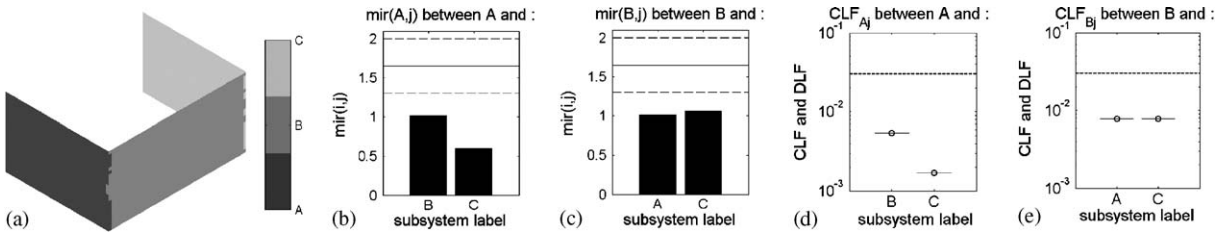

Fig. 20. (a) Substructuring of the three plates structure into 3 subsystems; (b) mir(i,j) indices between subsystems A and j ($j = B, C$); (c) mir(i,j) indices between subsystems B and j ($j = A, C$); (d) –○– coupling loss factors between subsystems A and j ($j = B, C$), - - -: damping loss factors; (e) –○– coupling loss factors between subsystems B and j ($j = A, C$), - - -: damping loss factors; 500 Hz third octave band, damping: 3%, CLF are calculated using Energy Influence Coefficients and inverse SEA.

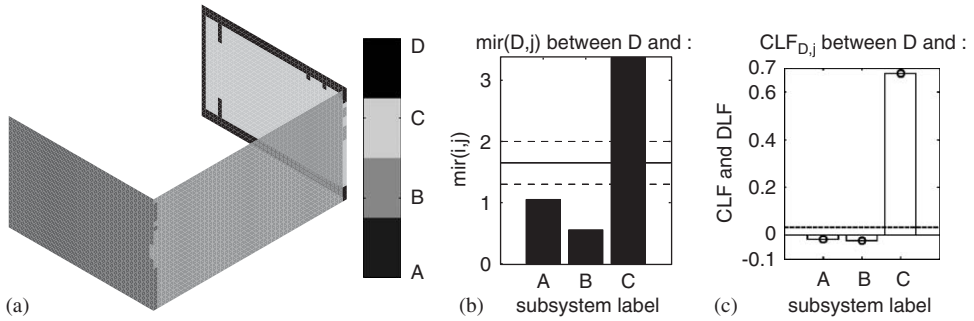

Fig. 21. (a) Substructuring of the three plates structure into 4 subsystems; (b) mir(i,j) indices between subsystems D and j ($j = A, B, C$); (c) –○– coupling loss factors between subsystems D and j ($j = A, B, C$), - - -: damping loss factors of subsystems. 500 Hz third octave band, damping: 3%, CLF are calculated using Energy Influence Coefficients and inverse SEA.

mir(i,j) value can be interpreted as a measure of dissimilarity between behaviors of two subsystems under some different excitations. The mir(i,j) value should decrease when distance between two subsystems or damping increases. Thanks to Figs. 20(d) and (e), one can remark that CLFs follow the same tendencies as the mir(i,j) index. In particular, one can verify that η_{AB} is higher than η_{AC} (indirect CLF) as predicted by mir index. Moreover, as mir(B,A) and mir(B,C), η_{BA} and η_{BC} are almost equal. CLF are all lower than damping loss factor (3%).

- In the case of four subsystems (Fig. 21(a)), the cluster analysis gathers elements near boundaries of plate C in the new subsystem D. However, mir(C,D) indicates that subsystems C and D have too similar behaviors to be considered as SEA subsystems. In that case, η_{DC} is particularly high (higher than 1 while damping loss factor is 0.03) and others CLF (η_{DA} and η_{DB}) are negative indicating that SEA assumptions are not respected.

It is demonstrated that the mir(i,j) index can be used as an indicator of coupling strength between two subsystems i and j. As seen in Figs. 19–21, the limit of SEA validity is relevant in the case of an assembly of three plates.

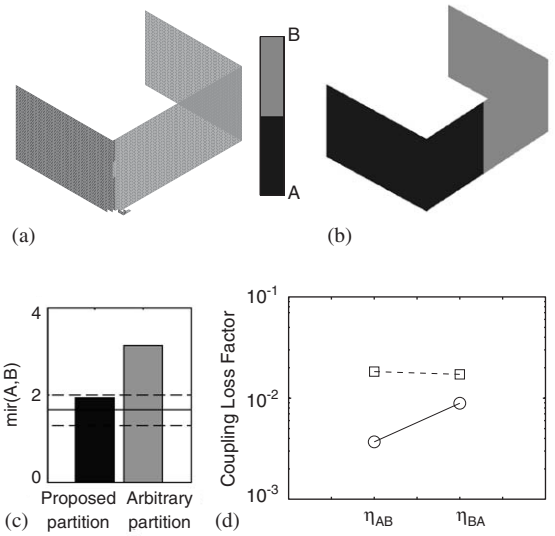

Fig. 22. Comparison between the proposed partition (a) and an arbitrary one (b) into 2 subsystems. (c) comparison between mir(A, B) of the proposed partition and the one of the arbitrary partition and (d) coupling loss factors in each case, –○–: proposed partition, –□– arbitrary partition. 500 Hz third octave band, damping: 3%, CLF are calculated using Energy Influence Coefficients and inverse SEA.

To verify that cluster analysis finds the best partition into k subsystems, two different partitions are compared in Fig. 22 in the case of two subsystems. The partition proposed by the present method is compared to an arbitrary one. In both cases, the MIR index and CLFs are calculated.

One can notice on Fig. 22(c) that the MIR index of the arbitrary partition is higher than the one of the proposed partition. This indicates that, in the case of the arbitrary partition, behaviors of subsystems are more similar. Fig. 22 shows that CLFs are higher for the arbitrary partition as assumed by MIR index. Using MIR index, cluster analysis finds the partition into k-subsystems which maximize the behavior dissimilarity between subsystems.

6. Complex test case substructuring

6.1. 500 Hz third octave band

Complex test case described in this section is presented in Fig. 23. It is composed of a thin shell having flat and curved parts, some connections are spot welded.

Six excitation points have been chosen to apply the substructuring method. Locations of the excitations are presented in Fig. 23. The substructuring was done, in a first step, for 500 Hz third octave and for a moderate damping coefficient (5%).

The MIR analysis presented in Fig. 24 shows that the best substructuring found by the algorithm is divided into two subsystems. In addition, a MIR value lower than unity indicates that

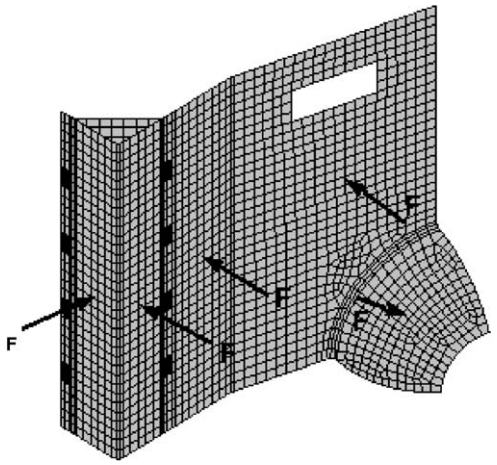

Fig. 23. Mesh and location of excitations for the complex test case.

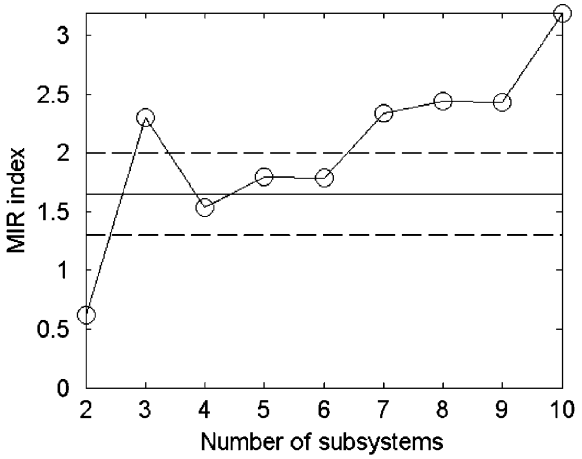

Fig. 24. MIR as a function of number of subsystems for the complex test case for 500 Hz third octave band.

subsystems have dissimilar enough behaviors to be considered as SEA subsystems. The resulting partitions into two and three subsystems are shown in Figs. 25 and 26.

In the case of three subsystems, the substructuring follow physical limits and detect spot welded plate as a subsystem. However, the MIR index indicates that behaviors of subsystems *B* and *C* are too similar to consider spot welded plate as an SEA subsystem.

6.2. 1000 Hz third octave band

In order to see how the substructuring depends on frequency, 1000 Hz third octave band was considered. Fig. 27 emphasizes that the test case could be divided into 2, 3 or 5 subsystems respecting criterion MIR < 1.3 indicating SEA validity. This means that three partitions are

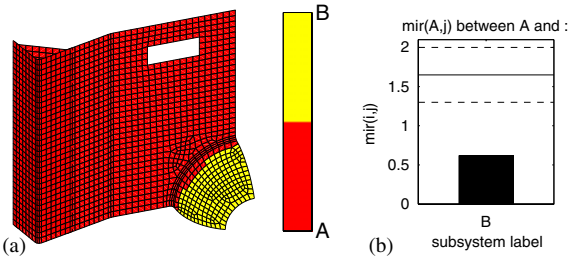

Fig. 25. (a) Sub-structuring into 2 subsystems for 500 Hz third octave band and (b) mir(i,j) indices between subsystems A and B.

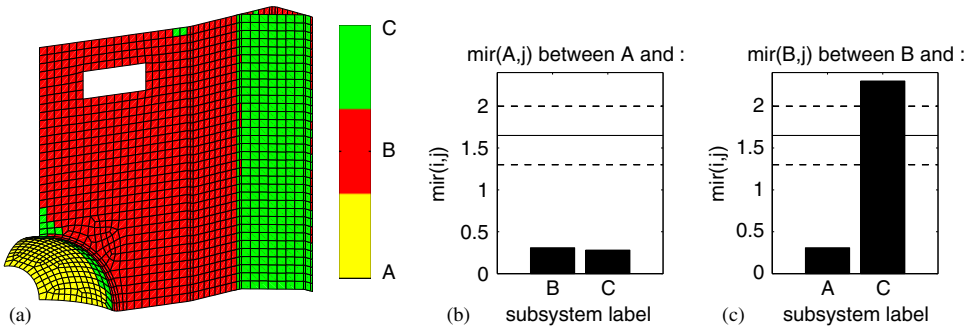

Fig. 26. (a) Sub-structuring into 3 subsystems for 500 Hz third octave band; (b) mir(i,j) indices between subsystems A and j ($j = B, C$) and (c) mir(i,j) indices between subsystems B and j ($j = A, C$).

possible and that some subsystems could be divided into smaller subsystems. Figs. 28–31 show partitions into 2–5 subsystems for 1000 Hz third octave band.

For the two subsystems case, the substructuring is similar to the one obtained for 500 Hz third octave band.

Fig. 29(a) shows that the structure can be divided into three subsystems, spot welded plate can now be considered as an SEA subsystem. When increasing the number of subsystems, the substructuring becomes more detailed but some subsystems have too similar behaviors and cannot be considered as SEA subsystems. For example, in Fig. 31(a), the mir(i,j) value between subsystems B and D is higher than the upper limit of validity.

Comparing partitions obtained in both third octave bands, one can see that evolution of the substructuring with frequency is weak, even if the number of subsystems that can be considered in SEA analysis tends to increase.

7. Conclusion

Substructuring is a basic step for applying SEA. For plates, some criteria were proposed to help this operation but for more complicated structures the problem was open. In this paper, a tool for

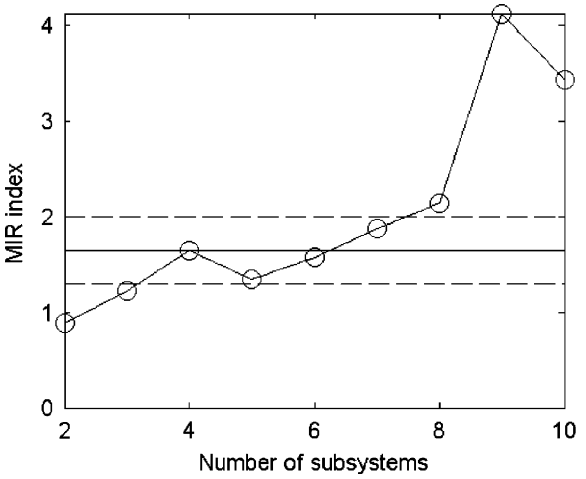

Fig. 27. MIR as a function of number of subsystems for the complex test case for 1000 Hz third octave band.

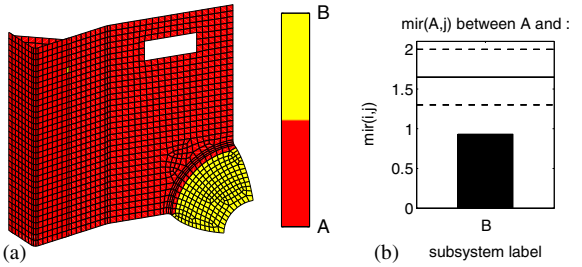

Fig. 28. (a) Sub-structuring into 2 subsystems for 1000 Hz third octave band and (b) mir(i,j) indices between subsystems A and B.

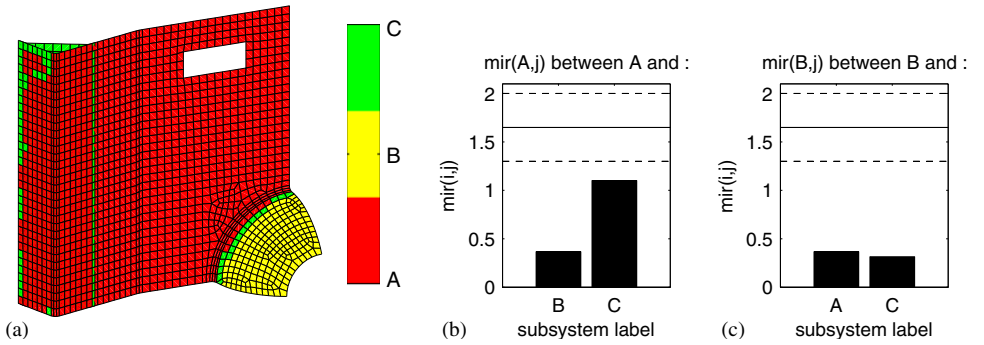

Fig. 29. (a) Sub-structuring into 3 subsystems for 1000 Hz third octave band; (b) mir(i,j) indices between subsystems A and j ($j = B, C$) and (c) mir(i,j) indices and between subsystems B and j ($j = A, C$).

substructuring was developed using energy transfer functions and cluster analysis. First of all, the importance of taking into account total energy rather than kinetic energy has been proved. In effect, assumption of equality between kinetic and strain energies at any point of the structure can

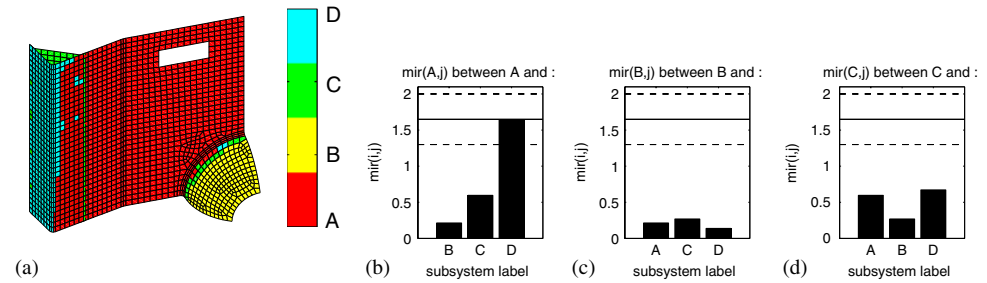

Fig. 30. (a) Sub-structuring into 4 subsystems for 1000 Hz third octave band; (b) mir(i,j) indices between subsystems A and j $(j = B, C, D)$; (c) mir(i,j) indices and between subsystems B and j $(j = A, C, D)$ and (d) mir(i,j) indices and between subsystems C and j $(j = A, B, D)$.

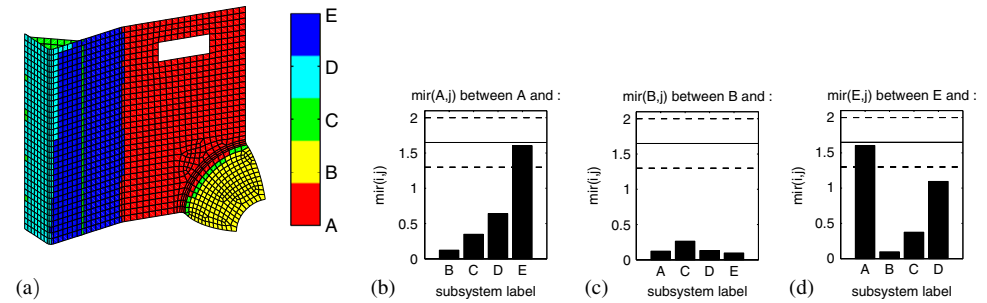

Fig. 31. (a) Sub-structuring into 5 subsystems for 1000 Hz third octave band; (b) mir(i,j) indices between subsystems A and j $(j = B, C, D, E)$; (c) mir(i,j) indices and between subsystems B and j $(j = A, C, D, E)$ and (d) mir(i,j) indices and between subsystems E and j $(j = A, B, C, D)$.

be quite wrong, especially at low frequency and for curved structures. For high frequency, the assumption become more and more accurate.

For the proposed method of substructuring, a database of N energy transfer functions matrices must be constructed experimentally or numerically. For each excitation, a projection on the P first principal components was done in order to describe each transfer function with P independent parameters. Using a classification algorithm, a substructuring with different number of subsystems is carried out. An index (MIR) has been established in order to indicate the best number of subsystems.

Substructuring of an assembly of three plates demonstrated that the minimal number of excitations spread over the structure can be estimated to $X - 1$, if X is the number of subsystems, in addition, the substructuring is stable for number of excitations higher than $X - 1$.

It has been also demonstrated that mir(i,j) index between subsystems i and j follows the same tendencies as CLFs between subsystems. The mir(i,j) index is correlated to coupling strengths between subsystems. Substructuring for different frequency bands have been carried out for a complex thin shell structure comprising flat and curved panels and welded points. It has been found that the substructuring slowly changes with frequency.

One has to notice that the present method only proposes a substructuring which should be suitable for SEA applications. However, an a posteriori validation of the corresponding SEA model has to be carried out.

References

[1] R.H. Lyon, R.G. Maidanik, Power flow between linearly coupled oscillators, *Journal of the Acoustical Society of America* 34 (1962) 623–639.
[2] P.W. Smith, Response and radiation of structural modes excited by sound, *Journal of the Acoustical Society of America* 34 (5) (1962) 640–647.
[3] R.S. Langley, A derivation of the coupling loss factors used in statistical energy analysis, *Journal of Sound and Vibration* 141 (2) (1990) 207–219.
[4] B.R. Mace, The statistical energy analysis of two continuous one-dimensional subsystems, *Journal of Sound and Vibration* 166 (3) (1993) 429–461.
[5] S. Finnveden, Ensemble averaged vibration energy flows in a three-element structure, *Journal of Sound and Vibration* 187 (3) (1995) 495–529.
[6] L. Maxit, J.-L. Guyader, Statistical power flow analysis between coupled subsystems, in: *INTER-NOISE 2001*, The Hague, Netherlands, 2001.
[7] L. Maxit, J.-L. Guyader, Estimation of SEA coupling loss factors using a dual formulation and FEM modal information, Part I: theory, *Journal of Sound and Vibration* 239 (5) (2001) 907–930.
[8] D.A. Bies, S. Hamid, In situ determination of loss and coupling loss factors by the power injection method, *Journal of Sound and Vibration* 70 (2) (1980) 187–204.
[9] F.J. Fahy, P.P. James, A study of the kinetic energy impulse response as an indicator of the strength of coupling between SEA subsystems, *Journal of Sound and Vibration* 190 (3) (1996) 363–386.
[10] F.J. Fahy, W.G. Price, *IUTAM Symposium on Statistical Energy Analysis*, ISVR, University of Southampton, 1997.
[11] S. Theodoridis, K. Koutroumbas, *Pattern Recognition*, Academic Press, New York, 1999.
[12] L. Kaufman, P.J. Rousseeuw, *Finding Groups in Data*, Wiley-Interscience Publication, New York, 1990.
[13] C. Zang, H. Grafe, M. Imregun, Frequency-domain criteria for correlating and updating dynamic finite element models, *Mechanical Systems and Signal Processing* 15 (1) (2001) 139–155.
[14] N. Totaro, Caractérisation de Sources Aérodynamiques et Sous-structuration Pour la Méthode SEA, Ph.D. Thesis, INSA, LYON, 2004.
[15] M.J.A. Berry, G. Linoff, *Data Mining Techniques, for Marketing, Sales and Customer Support*, Wiley, New York, 1997.
[16] J.M. Pena, J.A. Lozano, P. Larranaga, An empirical comparison of four initialization methods for the *K*-means algorithm, *Pattern Recognition Letters* 20 (1999) 1027–1040.
[17] S. Bandyopadhyay, U. Maulik, An evolutionary technique based on *k*-means algorithm for optimal clustering in $\mathbb{R}^n$, *Information Sciences* 146 (2002) 221–237.
[18] B.R. Mace, J. Rosenberg, The SEA of two coupled plates: an investigation into effects of subsystems irregularity, *Journal of Sound and Vibration* 212 (3) (1998) 395–415.
[19] R. Kothari, D. Pitts, On finding the number of clusters, *Pattern Recognition Letters* 20 (1999) 405–416.
[20] S. Gunter, H. Bunke, Validation indices for graph clustering, *Pattern Recognition Letters* 24 (2003) 1107–1113.
[21] N. Bolshakova, F. Azuaje, Cluster validation techniques for genome expression data, *Signal Processing* 83 (2003) 825–833.
[22] A.J. Keane, W.G. Price, *Statistical Energy Analysis: An Overview, with Applications in Structural Dynamics*, Cambridge University Press, Cambridge, 1997.
[23] W. Wöhle, T. Beckmann, H. Schreckenbach, Coupling loss factors for statistical energy analysis of sound transmission at rectangular structural slab joint, Part i, *Journal of Sound and Vibration* 77 (3) (1981) 323–334.

[24] E. Rebillard, Vibro-acoustique des Réseaux de Plaques: Modélisation, Hypersensibilité et Population de Structures, Ph.D. Thesis, INSA de Lyon, 1995.
[25] M. Ouisse, J.L. Guyader, An energy residual method for detection of the causes of vibration hypersensitivity, *Journal of Sound and Vibration* 260 (1) (2003) 83–100.
[26] J.L. Guyader, C. Boisson, C. Lesueur, Energy transmission in finite coupled plates, Part i: theory, *Journal of Sound and Vibration* 81 (1) (1982) 81–92.